Electronic Supplementary Material (ESI) for Journal of Materials Chemistry A.
This journal is © The Royal Society of Chemistry 2020

Electronic Supplementary Information

Boosting the electrochemical performance of hematite nanorods via quenching-induced metal single atom functionalization

Ming Su, [1] Zhenghui Pan, [2*] Yanan Chong, [1] Changchun Ye, [1] Xiaojing Jin, [1] Qingyuan Wu, [3] Zhao Hu, [1] Daiqi Ye, [1] Geoffrey I. N. Waterhouse, [4] Yongcai Qiu, [1, 5*] Shihe Yang[6]

[1]Guangdong Provincial Key Laboratory of Atmospheric Environment and Pollution Control, School of Environment and Energy, South China University of Technology, Guangzhou, 510006, China

[2]Institute of Flexible Electronics, Northwestern Polytechnical University, Xi'an 710072, People's Republic of China

[3]College of Chemistry and Chemical Engineering, Xiamen University, 361005, Xiamen, China

[4]School of Chemical Sciences, the University of Auckland, Auckland 1142, New Zealand

[5]State Key Laboratory of Luminescent Materials and Devices, South China University of Technology, Guangzhou, China

[6]School of Chemical Biology and Biotechnology, Peking University Shenzhen Graduate School, Shenzhen, China

E-mail: msepz@nus.edu.sg; ycqiu@scut.edu.cn

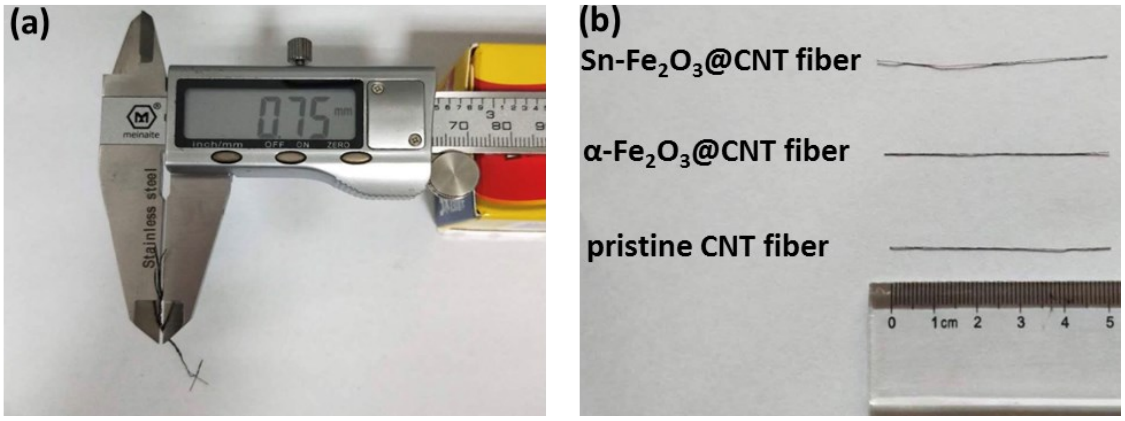

Figure S1. (a) The diameter of six CNT fibers. (b) The digital image of pristine CNT fiber, *α*-Fe_2O_3@CNT fiber, and Sn-Fe_2O_3@CNT fiber.

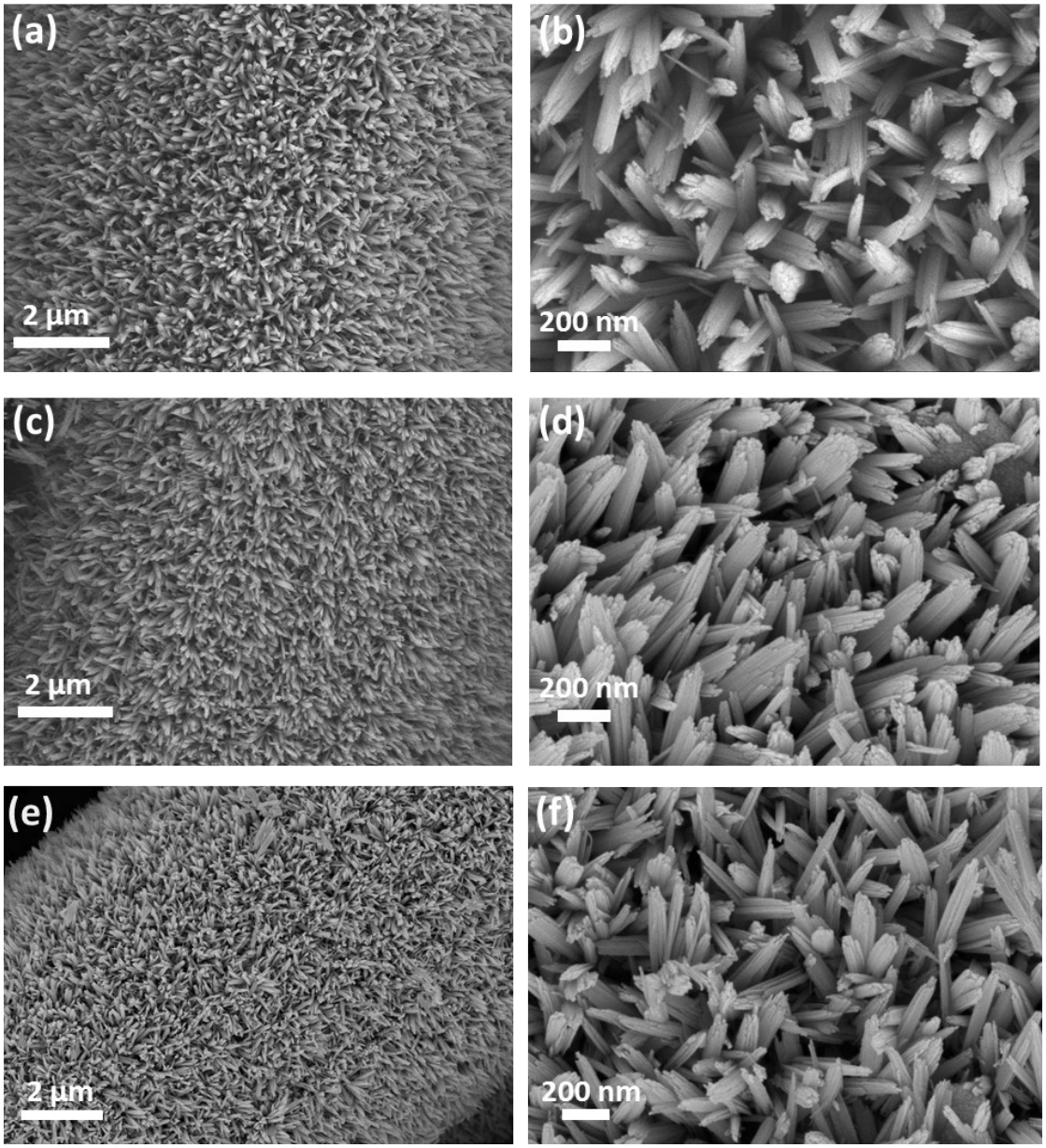

Figure S2. SEM images of (a, b) α-Fe_2O_3@CNT fiber, (c, d) DIW-Fe_2O_3@CNT fiber, and (e, f) Sn-Fe_2O_3@CNT fiber.

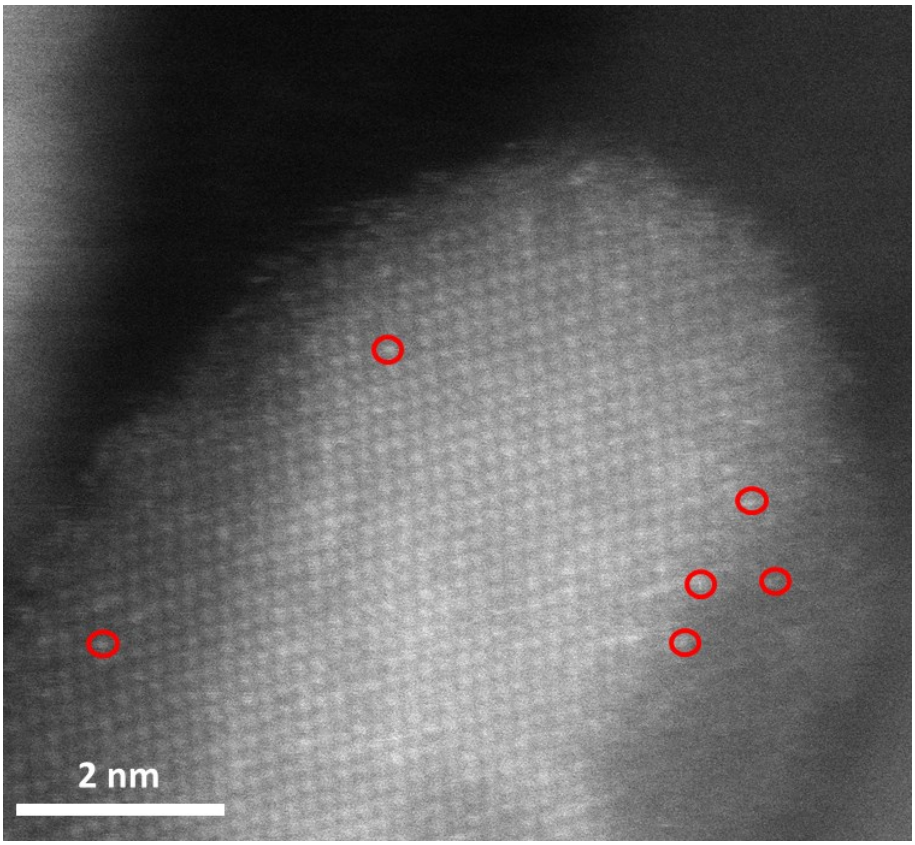

Figure S3. HAADF-STEM image of isolated Sn single atoms redistributed across the nanorod support.

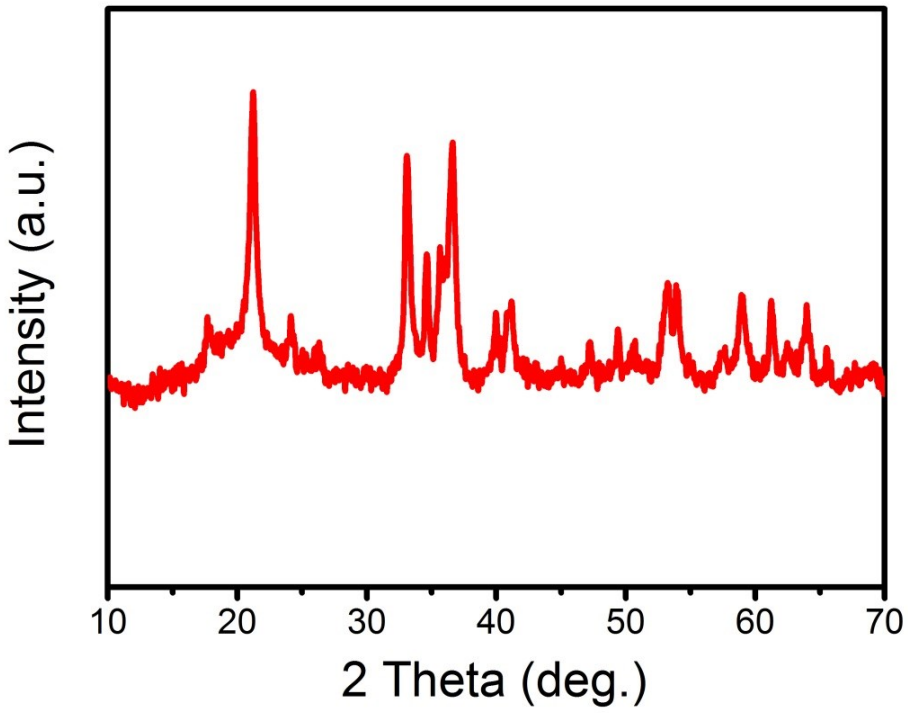

Figure S4. XRD pattern of the FeOOH@CNT fiber precursor.

The position and relative intensities of diffraction peaks in the XRD pattern closely match the JCPDS card for FeOOH (# 75-1594). [1]

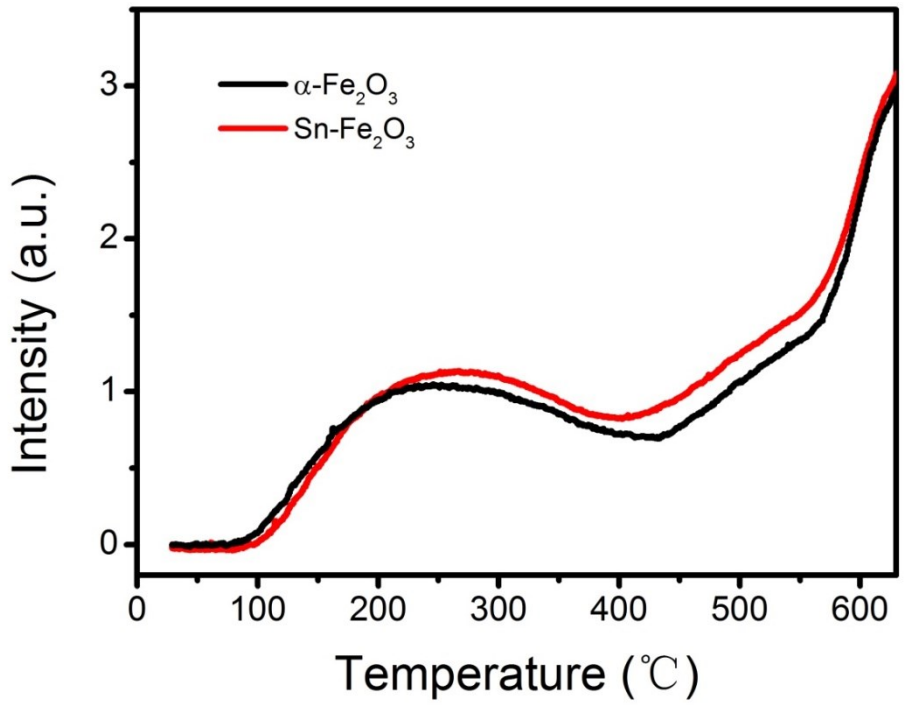

Figure S5. O_2-TPD profiles of α-Fe_2O_3@CNT fiber and Sn-Fe_2O_3@CNT fiber.

The nature of the surficial oxygen related to the conductivity of the electrode material and the form of surface adsorbed oxygen species may change via the following transformation reactions: O_2 (ad) → O^{2-} (ad) → O^- (ad) → O^{2-} (ad/lattice). The first peak (~250 ℃) represents the desorption of physically adsorbed oxygen. The second peak (~500 ℃) is related to the desorption of the chemically adsorbed species O^{2-} (and/or O^-) formed by the adsorbed oxygen on the oxygen vacancies. The third peak (< 600 ℃) signifies the desorption of lattice oxygen. It can be seen from the Figure S5 that the area of the second peak increases after quenching in the solution of $SnCl_4$, which means an increase in oxygen vacancies.

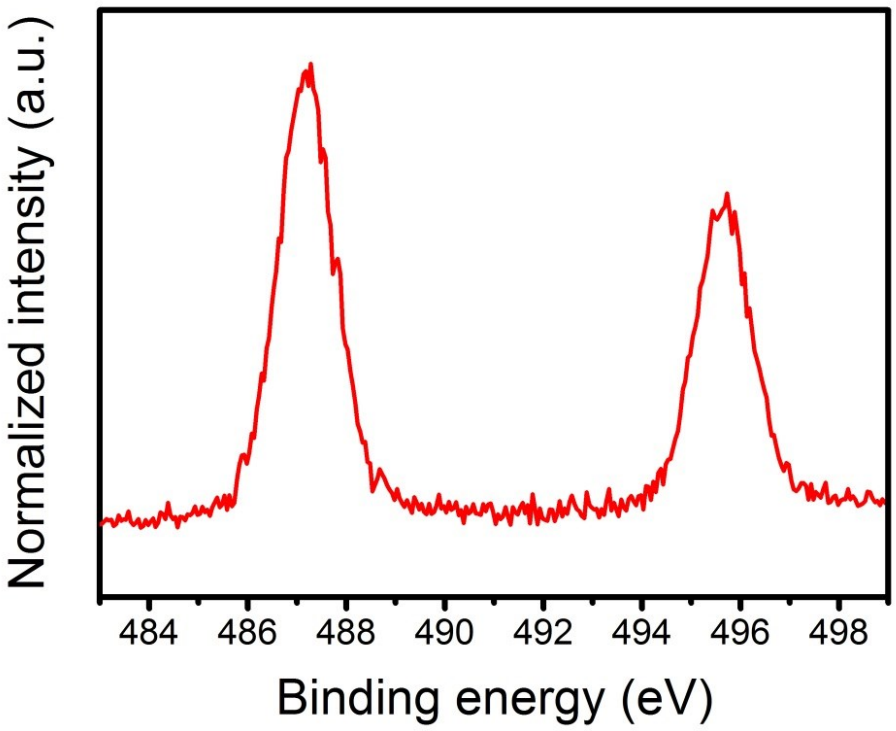

Figure S6. Sn 3d core-level XPS spectrum for the Sn-Fe_2O_3 @CNT fiber.

From Figure S6, it can be clearly seen that the Sn 3d peak in the XPS survey spectrum (binding energy is located at 487.19 and 495.63 eV correspond to the characteristic Sn $3d_{3/2}$ and Sn $3d_{5/2}$ peaks of Sn^{4+}), evidencing the existence of Sn.[2]

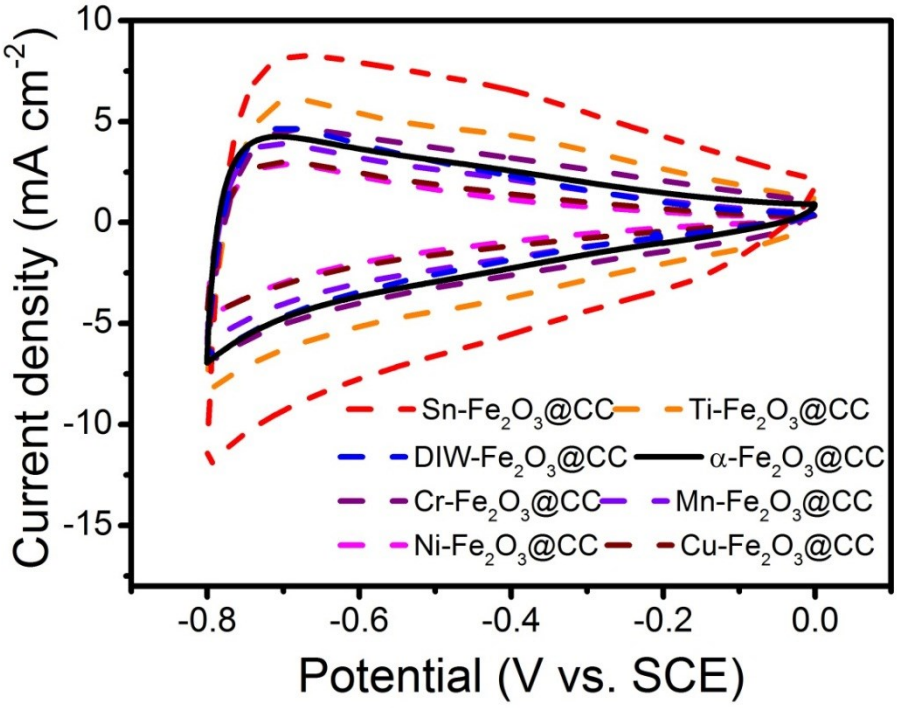

Figure S7. CV curves for Sn-Fe_2O_3@CC, Ti-Fe_2O_3@CC, DIW-Fe_2O_3@CC, α-Fe_2O_3@CC, Cr-Fe_2O_3@CC, Mn-Fe_2O_3@CC, Ni-Fe_2O_3@CC, and Cu-Fe_2O_3@CC electrodes collected in 5 M LiCl at a scan rate of 100 mV s^{-1}.

Because the low mass loading of the CNT fiber, it is difficult to reflect the changes of capacitance by doping other ions (the effect is not obvious). Therefore, carbon cloth is used to test the sample doping other ions. Carbon cloth (CC) and CNT fiber only serve as the current collects, and will not affect the performance of working electrodes.

In this work, α-Fe_2O_3@CC electrodes were quenched in aqueous solutions of $SnCl_4$, $TiCl_4$, deionized water (DIW), $CrCl_3$, $MnCl_2$, $CuCl_2$, and $NiCl_2$, to produce the samples denoted as Sn-Fe_2O_3@CC, Ti-Fe_2O_3@CC, DIW-Fe_2O_3@CC, α-Fe_2O_3@CC, Cr-Fe_2O_3@CC, Mn-Fe_2O_3@CC, Ni-Fe_2O_3@CC, and Cu-Fe_2O_3@CC respectively. Figure S7 shows that quenching α-Fe_2O_3@CC in DIW caused no change in the capacitance, whereas quenching in the solutions of different metal salts dramatically altered the capacitance. The data conclusively demonstrates that quenching α-Fe_2O_3 in the presence of aqueous metal salts

introduces metal single atoms, thus changing the conductivity (Figure S8) and capacitance of the material. Interestingly, the capacitance of α-Fe_2O_3@CC loaded with divalent MAS decreased when compared to the pristine α-Fe_2O_3@CC, while decorated with high valence (M^{3+} or M^{4+}) ions increase the conductivity and capacitance. We tentatively propose that the charge distribution on the surface of α-Fe_2O_3 changes after M^{2+} decoration, such that the electron donating ability of the material becomes weak. Conversely, for M^{4+} decoration, the capacitance increased greatly, suggesting an enhancement in electron transfer performance.

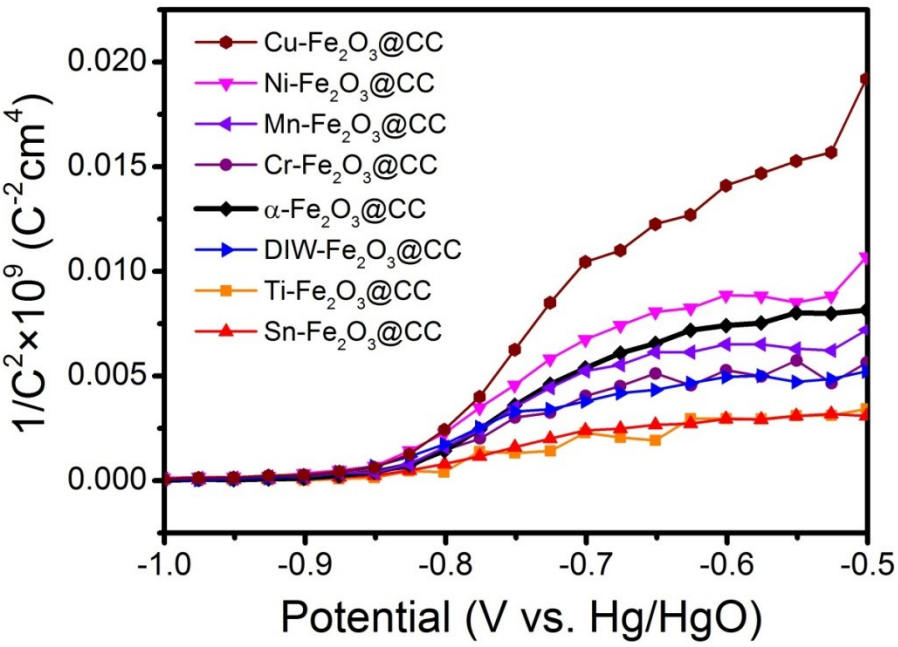

Figure S8. Mott-schottky curves for Sn-Fe_2O_3@CC, Ti-Fe_2O_3@CC, and DIW-Fe_2O_3@CC, α-Fe_2O_3@CC, Cr-Fe_2O_3@CC, Mn-Fe_2O_3@CC, Ni-Fe_2O_3@CC, and Cu-Fe_2O_3@CC electrodes in 1M NaOH at a frequency of 1 kHz.

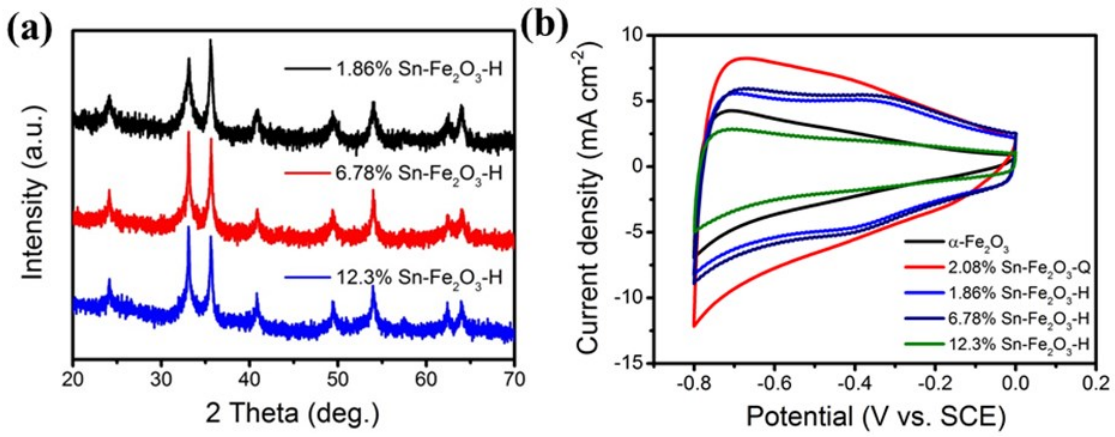

Figure S9. (a) Powder XRD patterns and (b) CV curves for 1.86, 6.78, 12.3% Sn-Fe_2O_3-H

The powder XRD pattern of the 1.86, 6.78, 12.3% Sn-Fe_2O_3-H@CNT fiber (Sn-Fe_2O_3@CNT fiber prepared by hydrothermal method) sample matched the JCPDS card for hematite (# 33-0664) implying that the hydrothermal not alter the structure of the supported α-Fe_2O_3.[3] CV curves for hydrothermal and quenching sample collected at a sweep rate of 100 mV s^{-1} are shown in Figure S9b. The current density of the 2.08% Sn-Fe_2O_3-Q electrode is significantly higher than that of 1.86, 6.78, 12.3% Sn-Fe_2O_3-H electrodes.

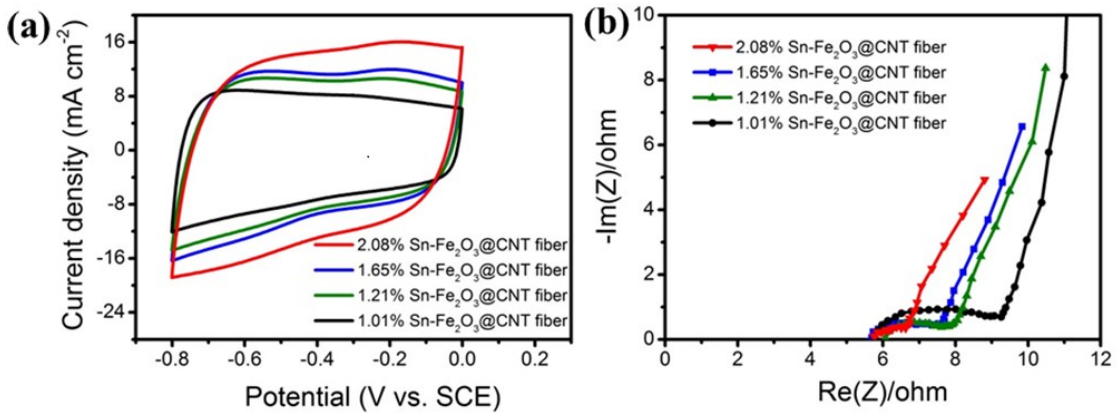

Figure S10. (a) CV curves and (b) Nyquist plots of Sn-Fe_2O_3@CNT fiber electrodes in different amount of Sn single atoms.

To investigate the influence of mass loading of Sn single atom on the electrochemical properties of the Sn-Fe_2O_3@CNT fiber electrodes, we changed the concentration of the quenching solution (0.001 M, 0.005 M, 0.05 M and 0.5 M, respectively) and obtained samples with different amount of doping (1.01%, 1.21%, 1.65% and 2.08%, respectively, which are examined from ICP-OES). CV curves for different concentrations of samples collected at a sweep rate of 100 mV s^{-1} are shown in Figure S10a. The current density of the 2.08% Sn-Fe_2O_3 electrode is significantly higher than that of 1.01%, 1.21% and 1.65% Sn-Fe_2O_3 electrodes and the corresponding capacitances are 120.9, 143.7, 158.4 and 199.1 mF cm^{-2}, respectively. Such improved capacitance for 2.9% Sn-Fe_2O_3 electrode can be attributed that the high loading of Sn^{4+} single atom enhances electron and ion transfer between the fiber electrode and the electrolyte interface. Furthermore, the Nyquist plot shows the same result.

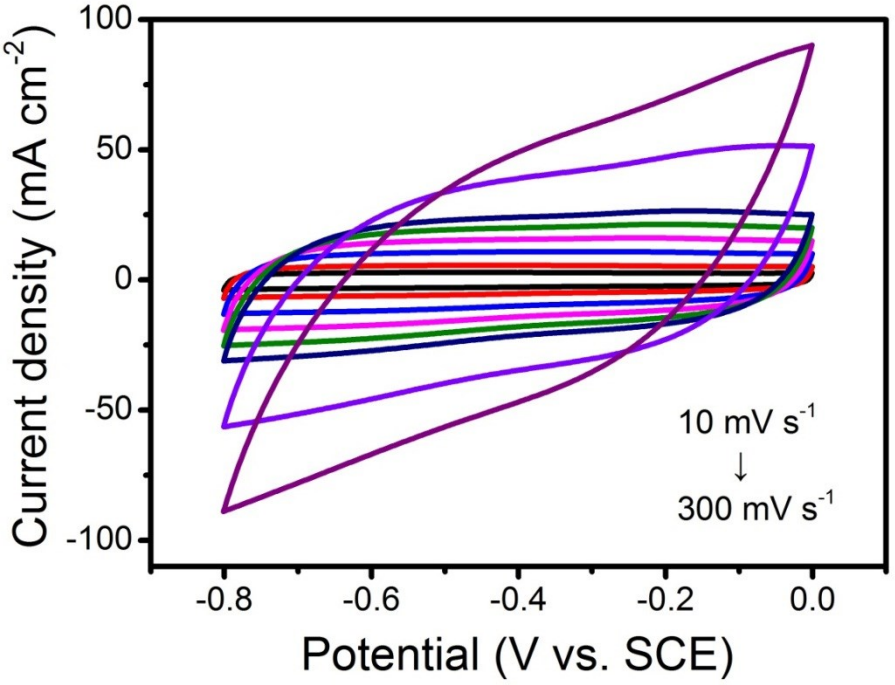

Figure S11. CV curves for the Sn-Fe_2O_3@CNT fiber electrode collected at various scan rates in 5 M LiCl.

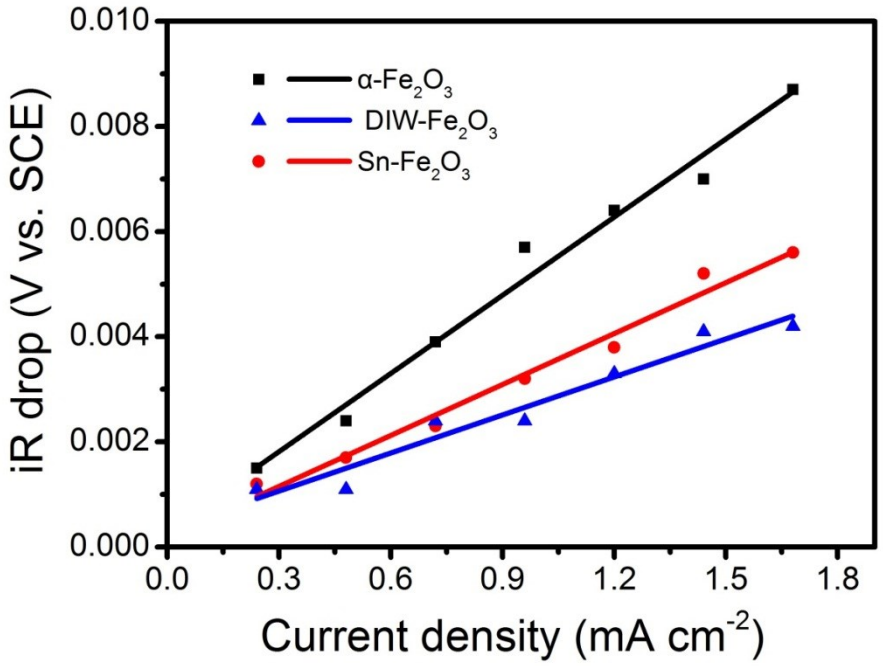

Figure S12. IR drop curves for the α-Fe_2O_3@CNT, DIW-Fe_2O_3@CNT and Sn-Fe_2O_3@CNT fiber electrodes collected at different current densities in 5M LiCl.

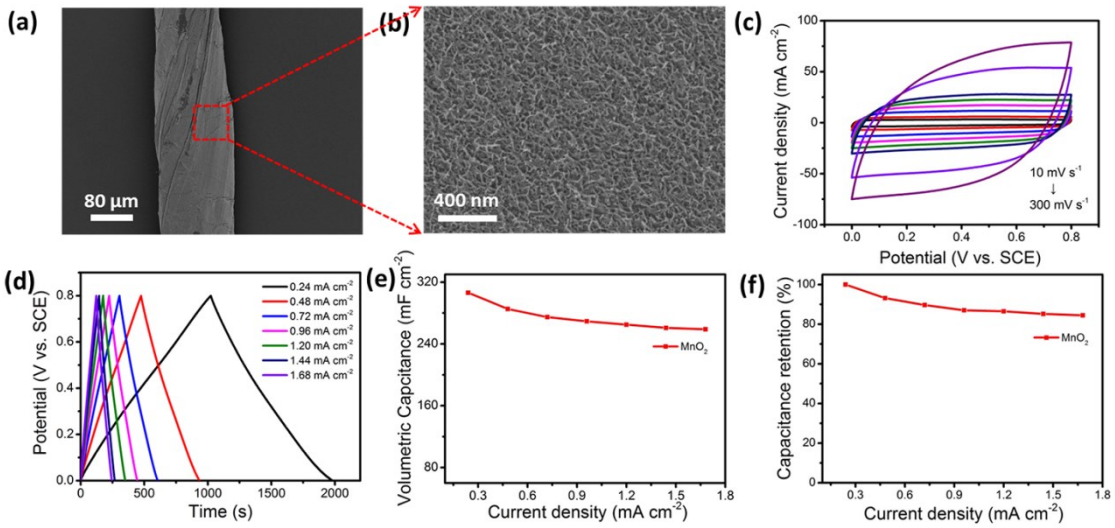

Figure S13. (a, b) SEM images of the MnO_2@CNT fiber electrode at different magnifications. (c) CV curves for the MnO_2@CNT fiber electrode collected at various scan rates. (d) GCD curves for the MnO_2@CNT fiber electrode collected at different current densities. (e) Specific areal capacitances at different current densities. (f) Capacitance retention at different current densities.

The SEM images of Figure S13a and b shows that the electrodeposited MnO_2 is very uniformly coated on the CNT fiber, forming a porous network structure with a large specific surface area. The CV and GCD curves in Figure S13c and d, respectively, are collected in the same standard three-electrode system in 5M LiCl aqueous electrolyte. The MnO_2@CNT fiber electrode exhibits excellent energy storage performance, evidenced by the CV curves which maintain a parallelogram shape as the scanning speed increased from 10 mV s^{-1} to 300 mV s^{-1}. This behavior is consistent with superior rate capacity performance. The GCD curves (Figure S13d) maintain an equilateral triangle shape with increasing current density, suggesting a comparable columbic efficiency and good reaction reversibility. The calculated areal capacitance of the MnO_2@CNT fiber electrode at different current densities is shown in Figure S13e. When the current density is 0.24 mA cm^{-2}, a maximum capacitance of 306.3 mF cm^{-2} is realized. Since this capacitance is a good match the Sn-Fe_2O_3@CNT fiber negative

electrode (Figure S14), the FSC constructed using the two different fiber electrodes will have good symmetry. Further, the MnO_2@CNT fiber electrode demonstrates excellent capacitance retention. When the current density reaches 1.68 mA cm^{-2}, a capacity of 84.45% is maintained (Figure S13f).

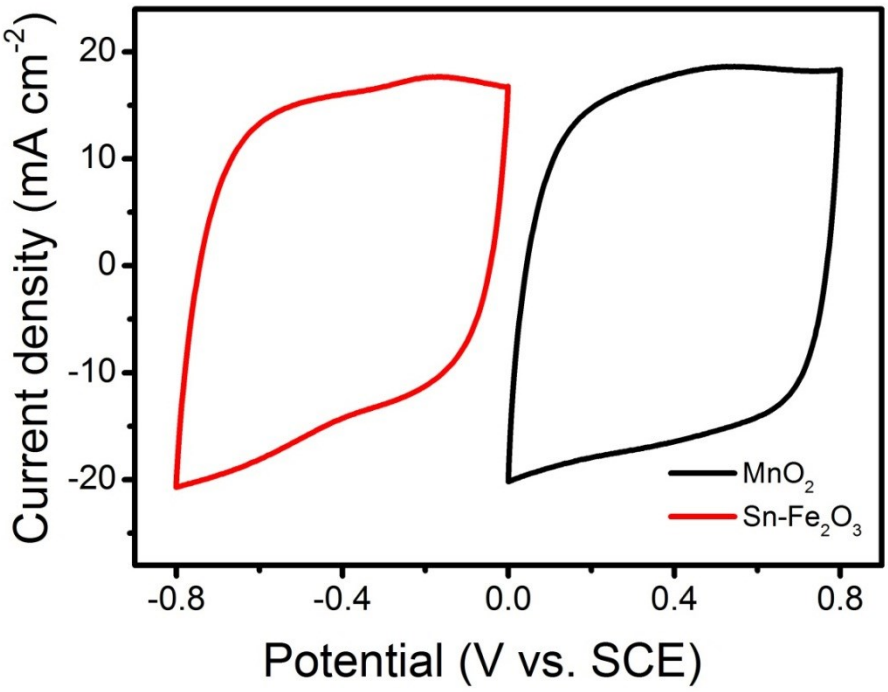

Figure S14. CV curves collected for MnO_2@CNT and Sn-Fe_2O_3@CNT fiber electrodes in 5M LiCl at a scan rate of 100 mV s^{-1}.

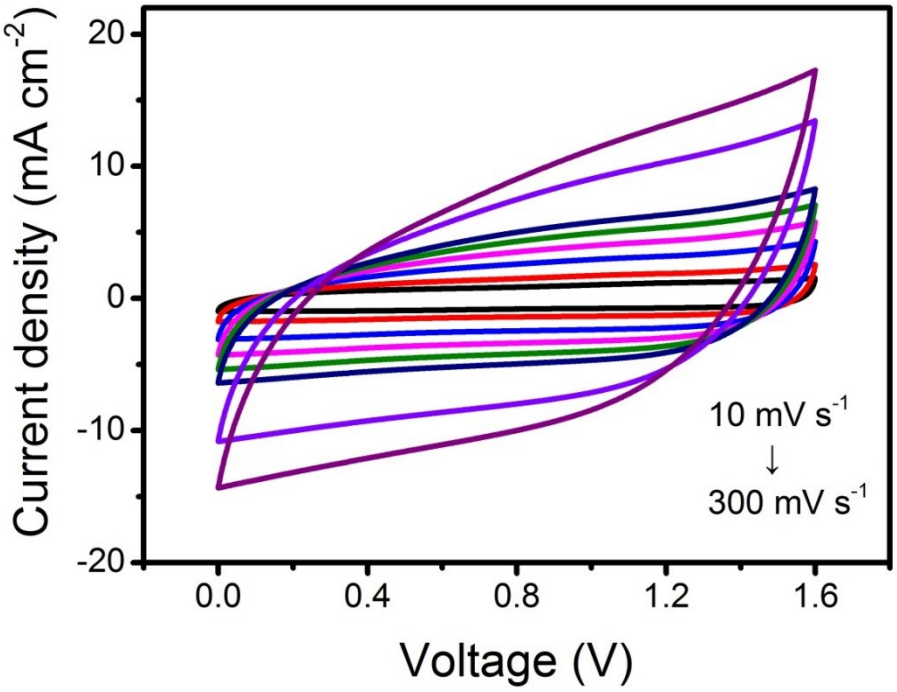

Figure S15. CV curves for all-solid-state Sn-Fe_2O_3@CNT//MnO_2@CNT FSC collected at various scan rates over a voltage window of 1.6 V.

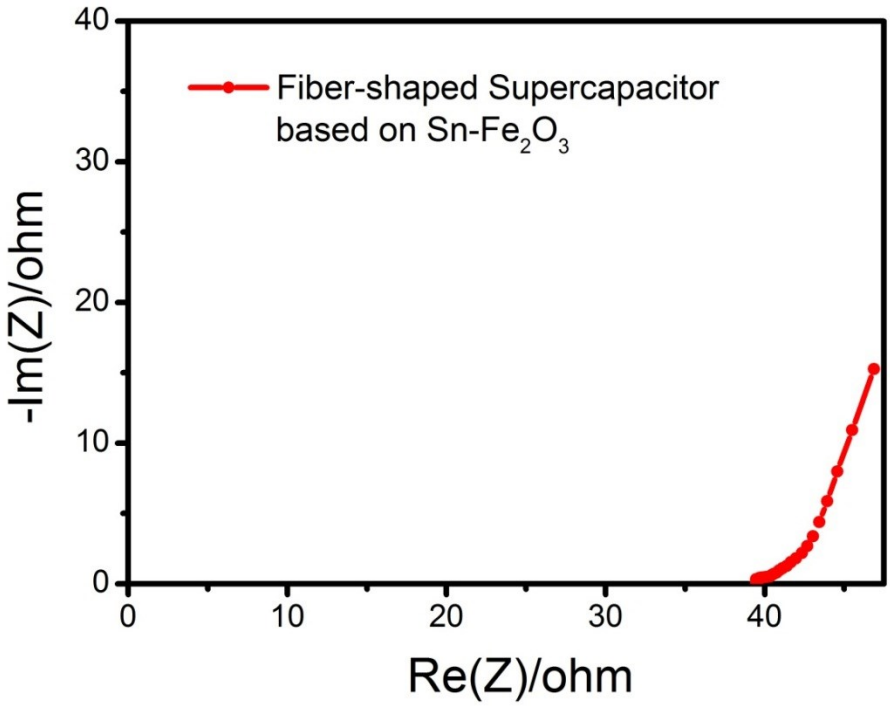

Figure S16. Nyquist plot for all-solid-state Sn-Fe_2O_3@CNT//MnO_2@CNT FSC.

Table S1. The content of Sn in Sn-Fe_2O_3@CNT fiber according to the ICP-OES measurement.

Sample	Sn (mg/Kg)	Sn (wt. %)
2.08%-Sn-Fe_2O_3-Q	20769	2.08
1.86%-Sn-Fe_2O_3-H	18622	1.86
6.78%-Sn-Fe_2O_3-H	67766	6.78
12.3%-Sn-Fe_2O_3-H	122499	12.25
1.65%-Sn-Fe_2O_3-Q	16555	1.65
1.21%-Sn-Fe_2O_3-Q	12080	1.21
1.01%-Sn-Fe_2O_3-Q	10117	1.01

Table S2. The oxygen vacancies content of α-Fe_2O_3, DIW-Fe_2O_3 and Sn-Fe_2O_3 nanorods according to XPS measurement.

Sample	Fe^{2+} (709.8-710.5eV)	oxygen vacancies (531.2-531.8 eV)
α-Fe_2O_3	0.48	0.36
DIW-Fe_2O_3	0.60	0.41
Sn-Fe_2O_3	0.45	0.46

Table S3. EXAFS fitting parameters results for Sn-Fe_2O_3.

Sample	Path	CN	R (Å)	σ(Å^2)	ΔE_0 (eV)
Sn	Sn-Sn	6	3.07±0.021	0.009±0.001	4.94±0.64
Sn-Fe_2O_3	Sn-O	5.13±0.11	1.99±0.011	0.006±0.003	1.98±0.05
	Sn-Fe	1.05±0.09	3.24±0.007		
SnO_2	Sn-O	6.35±0.55	2.05±0.008	0.002±0.001	5.24±1.01
	Sn-Sn	3.42±1.32	3.71±0.007	0.000±0.002	

Table S4. Summarized electrochemical characterization data for different samples.

Sample	Flat-band potential (eV) [a)]	Donor density (cm^{-3}) [a)]
α-Fe_2O_3@CNT	-0.71	1.62×10^{19}
DIW-Fe_2O_3@CNT	-0.72	1.91×10^{19}
Sn-Fe_2O_3@CNT	-0.75	3.5×10^{19}

[a)]The flat-band potential and donor density are calculated from the Mott-Schottky curve (Figure 4e).

References

1. Y. Song, S. Qin, Y. Zhang, W. Gao and J. Liu, *J. Phys. Chem. C*, 2010, **114**, 21158-21164.
2. Y. Ling, G. Wang, D. A. Wheeler, J. Z. Zhang and Y. Li, *Nano letters*, 2011, **11**, 2119-2125.
3. P. Kumar, P. Sharma, R. Shrivastav, S. Dass and V. R. Satsangi, *Int. J. Hydrogen Energy*, 2011, **36**, 2777-2784.